frontiers in Materials

ORIGINAL RESEARCH
published: 24 March 2020
doi: 10.3389/fmats.2020.00060

Strain-Induced Modulation of Spin Configuration in $LaCoO_3$

Linxia Wang[1], Jieyu Liu[1], Minghui Wu[2], Hanming Wu[3], Kaixiang Li[3], Yuankai Shao[3], Zhenguo Li[3] and Weichao Wang[1]**

[1] College of Electronic Information and Optical Engineering, Tianjin Key Laboratory of Photo-Electronic Thin Film Device and Technology, Renewable Energy Conversion and Storage Center, Nankai University, Tianjin, China, [2] Center for Advanced Marine Materials and Smart Sensors, Minjiang University, Fuzhou, China, [3] National Engineering Laboratory for Mobile Source Emission Control Technology, China Automotive Technology and Research Center, Tianjin, China

For oxides with octahedron ligand field, such as perovskite, spinel, and mullite, unit occupancy of e_g orbital plays a key role in governing the catalytic performance of oxygen redox in the application of renewable energy storage and conversion. The magnetic configurations greatly influence the e_g occupancy of these oxides. In this work, using the perovskite $LaCoO_3$ as an example, we use density functional theory (DFT) calculations to achieve an intermediate spin configuration corresponding to unit-like e_g occupancy via strain schemes. We determined that the introduction of strain by changing lattice constants effectively tailors electronic configurations. The low-spin ($t_{2g}^6 e_g^0$), intermediate-spin ($t_{2g}^5 e_g^1$), and high-spin ($t_{2g}^4 e_g^2$) configurations are obtained with the strain $\gamma < 1.0\%$, $1.0\% \leq \gamma < 4.0\%$, and $\gamma \geq 4.0\%$, respectively. To obtain the e_g unit occupancy practically, Ba with a larger ionic radius relative to La is inserted into A site to replace La elements, introducing tensile strain to the pristine $LaCoO_3$. The Ba substitution of La leads to the desirable spin configuration with the unit-like e_g occupancy. These findings provide a scenario on how to precisely control the unit occupancy of e_g via defect induced strain.

Keywords: cubic $LaCoO_3$, spin configurations, strain, substitutional defect, density functional theory

OPEN ACCESS

Edited by:
Zhenhai Xia,
University of North Texas, United States

Reviewed by:
Zhao-Qing Liu,
Guangzhou University, China
Gang Zhao,
University of Jinan, China

****Correspondence:***
Zhenguo Li
lizhenguo@catar.ac.cn
Weichao Wang
weichaowang@nankai.edu.cn

Specialty section:
This article was submitted to Energy Materials, a section of the journal Frontiers in Materials

Received: *17 January 2020*
Accepted: *26 February 2020*
Published: *24 March 2020*

Citation:
Wang L, Liu J, Wu M, Wu H, Li K, Shao Y, Li Z and Wang W (2020) Strain-Induced Modulation of Spin Configuration in $LaCoO_3$. Front. Mater. 7:60. doi: 10.3389/fmats.2020.00060

INTRODUCTION

The development of oxygen catalysts plays a significant role in accelerating the oxygen redox reaction in energy storage and conversion devices. In relation to the discovery of highly efficient non-precious catalysts like oxide, one needs to perform in-depth access with regard to the relation between the crystal structure and the catalytic property. Electronic structures are the fundamental origin of excellent catalytic performances of materials (Suntivich et al., 2011a; Maitra et al., 2013; Li et al., 2016; Gani and Kulik, 2018; Wang et al., 2019a; Zhang et al., 2019; Xu et al., 2020). For perovskites, e_g orbital occupancy is one of the effective descriptors in illustrating catalytic behavior. In the 1970s, Matsumoto et al. (1977b) first proposed that e_g orbital features in bulk transition metal oxides could reflect the catalytic trend of oxygen reduction reaction (ORR). They pointed out that the formation and filling of a σ* band due to the interaction between e_g orbital of transition metal

ion and oxygen molecular orbital greatly affects the ORR activity (Matsumoto et al., 1977a,b). To date, this bulk descriptor has been widely used to understand and predict the catalytic performance of oxides. For instance, Wei et al. (2017) demonstrated that e_g occupancy of the active cation in octahedral sites is an efficient descriptor for the ORR/OER activities of spinel. They proposed that a moderate e_g filling ($e_g \approx 1$) at the octahedral site can optimize ORR/OER activity. A similar conclusion in terms of e_g filling was further drawn in double perovskites (Jiang et al., 2018).

In 2010, Shao-Horn and colleagues presented research that confirmed that the e_g filling of transition metal ions in surface accounts for the ORR/OER activity of perovskites (Suntivich et al., 2011a,b). They found that maximum activity can be achieved when e_g orbital is occupied by a single electron for OE(R)R reaction. In contrast to traditional band theory, they assumed that a localized e_g electron in an orbital directed toward an O_2 molecule from the surface B cations is essential for ORR/OER. The use of the surface e_g filling promotes the accurate prediction of catalytic activities for ORR/OER over oxides. The probe of surface e_g filling is very challenging even to date. Compared with hard X-ray absorption spectroscopy (XAS), the soft XAS in principle enables one to access the surface properties depending on the incident energy and the corresponding modes. Shao-Horn and colleagues (Hong et al., 2015) claimed that the e_g occupancy in their previous studies (Suntivich et al., 2011a,b) was estimated on the basis of the oxidation state and spin state derived from bulk-sensitive measurements, i.e., hard X-ray absorption and magnetometry. In 2018, in their other review (Kuznetsov et al., 2018), they also mentioned that the values of e_g fillings were estimated from *ex situ* measurements or obtained from computed binding energies of oxygenated species on the surface. Therefore, the surface e_g descriptor in current reports fails to be solid. It could be more reasonable to be a bulk descriptor. In any case, the importance of Shao-Horn's work reveals the relation between the e_g unit filling of bulk materials and the catalytic properties, even if the relation between bulk and surface remains inaccessible so far. Therefore, the e_g unit filling of bulk, rather than the surface, is the key to ensure high catalytic efficiency.

Perovskite oxides contain different spin configurations in a given system. For instance, $LaCoO_3$ exhibits three spin configurations of low ($t_{2g}^6 e_g^0$), intermediate ($t_{2g}^5 e_g^1$), and high spin ($t_{2g}^4 e_g^2$). For e_g^1, the unit occupancy contributes to a moderate hybridization between d_{z^2} and oxygen 2*p* orbital to achieve an optimized catalytic activity. To date, much effort has been paid to improve the catalytic activity of $LaCoO_3$ by tuning its electronic structures. For example, the spin state of Co was adjusted by changing particle sizes of $LaCoO_3$ or doping Fe atom at Co sites to boost the catalytic performance (Zhou et al., 2016; Duan et al., 2017). However, the precise control of the specific intermediate spin configuration is still challenging. In principle, strain technology, defects, and interfacing are alternative schemes (Zhao et al., 2018, 2019, 2020a), among which the strain technology is one of the widely adopted schemes to tune electronic properties and thereby tailor the reactivity of materials. Mavrikakis et al. (1998) proposed that the strain changes the reactivity of transition metal surface by shifting the *d*-band center; this model is general and suitable for a number of metal surfaces to successfully explain chemical behaviors of materials under strain (Hammer et al., 1996, 1997; Holmblad et al., 1996; Kratzer et al., 1996; Hammer and Norskov, 2000; Liu et al., 2011). In addition, for the widely used platinum catalyst, a compressive strain of 1% can induce activity enhancement of more than 300% for ORR (Strasser et al., 2010; Escudero-Escribano et al., 2012; Asano et al., 2016; Escudero-Escribano et al., 2016). Wang et al. (2019b) found that the control of the thickness of two-dimensional transition metal at atomic level can achieve fine-tuning intrinsic strain. Moreover, the activity of oxygen reduction and hydrogen evolution reactions can be improved by more than an order of magnitude relative to corresponding nanoparticle counterparts. For oxides, strain primarily impacts the orbital characteristics, like energy level arrangement of the *d* subset and its occupancy, and consequently, the catalytic properties. The different strain along in-plane and out-of-plain direction can remove degenerate of e_g orbital, and alter the occupancy of d_{z^2} (Freeland et al., 2011; Pesquera et al., 2012).

Although strain technology has been proven to be effective, the physics behind it remains inaccessible, and the modulation of e_g occupancy is not explored yet. Here, we use cubic $LaCoO_3$ as a model catalyst to systematically investigate the effect of strain on electronic configurations closely relevant for catalytic performance, such as *d*-band center and electron spin arrangements. We focus on the strain induced by modifying lattice in the absence of octahedral distortions. When the uniform strains were applied, the magnetic moment of Co atom showed step-like behavior versus strain ($\gamma < 1.0\%$, Mag_{Co}: 0.0 μ_B; $1.0\% \leq \gamma < 4.0\%$, Mag_{Co}: 1.406 μ_B; $\gamma \geq 4.0\%$, Mag_{Co}: 2.561 μ_B). The substitution of La by large-radius Ba introduces strain leading to the e_g unit-like occupancy. Significantly, the lower oxidation state of Ba compared with La leads to a magnetic moment localized at the Co atom in Ba substitution-modified $LaCoO_3$ larger than that of the equivalent strained defect-free $LaCoO_3$. This work provides insights into the precise control of e_g unit occupancy via defect induced strain.

COMPUTATIONAL MODELS AND SETUPS

All calculations are performed in the framework of spin-polarized density functional theory (DFT), using the projector-augmented wave (PAW) method (Kresse and Joubert, 1999), as implemented in VASP code (Kresse and Furthmüller, 1996). The exchange–correlation interaction is treated in the generalized gradient approximation (GGA) of Perdew, Burke, and Ernzerhof (PBE) (Perdew et al., 1996). To describe the electronic correlation effect of 3*d* electrons of Co element, the DFT+U method (Anisimov et al., 1991) with a U_{eff} of 2.8 eV was employed. The energy cutoff for the plane–wave basis is set to be 550 eV. The calculated lattice parameters of $LaCoO_3$ are a = b = c = 3.811 Å, which agree well with previous theoretical and experimental results (Ganguly and Vasanthacharya, 1986; Kushima et al., 2010; Rivadulla et al., 2013). A Monkhorst-Pack Γ-centered 11 × 11 × 11 k-point

mesh was used for Brillouin zone sampling. Accordingly, for the $2 \times 2 \times 2$ supercell, the $7 \times 7 \times 7$ k-point mesh was adopted. The magnitude of the force acting on each atom to be allowed to relax is less than 0.01 eV/Å.

The substitutional energy per Ba atom in $La_{1-x}Ba_xCoO_3$ with different composition x is defined as

$$E^{Ba}_{substitutional} = \frac{1}{x}(E_{La_{1-x}Ba_xCoO_3} - E_{LaCoO_3} + \frac{x}{2}E^{La_2O_3}_{bulk} - xE^{BaO}_{bulk} - \frac{x}{4}E_{O_2}),$$

where $E_{La_{1-x}Ba_xCoO_3}$ and E_{LaCoO_3} are the total energy of Ba substitution-modified $LaCoO_3$ and pristine $LaCoO_3$. $E^{La_2O_3}_{bulk}$, E^{BaO}_{bulk}, and E_{O_2} are the energy of bulk La_2O_3, bulk BaO, and oxygen gas, respectively.

RESULTS AND DISCUSSION

Electronic and Elastic Properties of $LaCoO_3$

Prior to exploring the effect of strain on the electronic properties of bulk $LaCoO_3$, it is necessary to first calculate the electronic structures with effective on-site coulomb-exchange interaction parameter U_{eff} varying from 1.0 to 4.6 eV. **Figure 1** presents the calculated bandgap of bulk $LaCoO_3$ (see **Figure 2A**) under different U_{eff}. It is found that the bulk $LaCoO_3$ exhibits metallic properties for $U_{eff} < 1.8$ eV. And, with the U_{eff} increasing beyond 1.8 eV, the bandgap occurs. When U_{eff} value of 2.8 eV was employed, a bandgap of 0.441 eV was observed which is in good consonance with experimental results (Chainani et al., 1992; Abbate et al., 1993; Arima et al., 1993). Therefore, we adopted the U_{eff} of 2.8 eV in the following discussions. As shown in **Figure 2B**, the degenerate 3*d* orbitals of the free Co atom are split into t_{2g} and e_g bands under the restriction of cubic symmetry of $LaCoO_3$. The valence bands and the conduction bands are attributed to t_{2g} and e_g, respectively. This indicates that six *d* electrons of trivalent Co ion fully occupied t_{2g} orbitals, agreeing well with non-magnetic ground states of $LaCoO_3$ (Abbate et al., 1993). Besides, there is significant hybridization O-2*p* and Co-3*d*, suggesting a strong covalent bond between Co and O. The empty states at the energy of 4.0 eV above Fermi level are the La 4*f* states. The Bader charge analysis suggests that the calculated charge transfer of La is $+2.071e$, close to its formal charges of $+3e$. The charge transfer of Co and O atom is $+1.355e$ and $-1.142e$, respectively. This deviation of the charge transfer from the corresponding formal charges $+3e$ and $-2e$ further confirms the covalent feature of Co–O bond. In our DFT analysis for the effect of strain on the spin arrangement of $LaCoO_3$, the strain is achieved by equally changing lattice parameters along with a, b, and c directions. The strain is evaluated by $\gamma = (a_s - a)/a \times 100\%$, where a_s and a are the lattice constants of strained and strain-free structure, respectively. The corresponding strain energy of $LaCoO_3$ is defined as $\Delta E = E_s - E$, where E_s and E denote the total energy of strained and strain-free structure, respectively. **Figure 2C** shows the curve of the strain energy ΔE of $LaCoO_3$ versus γ. The minimum ΔE occurs at $\gamma = 0$, corresponding to the unstrained system.

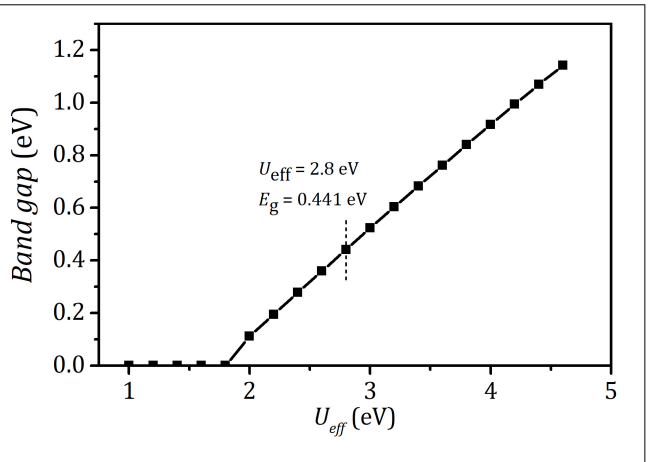

FIGURE 1 | Bandgap of bulk $LaCoO_3$ as a function of effective coulomb-exchange interaction parameter U_{eff} (1.0–4.6 eV).

To assess the strain effect on electronic configurations within a reasonable strain range, we first determined the ultimate strain of $LaCoO_3$ by calculating the strain–stress curve. It is evident that stress increases with strain and reaches a peak at 18%, as shown in **Figure 2C**. The ultimate strain of 18% suggests a good resistance to stress for $LaCoO_3$, which makes it possible to synthesize multicomponent perovskites by partially substituting La or Co, reflecting the diversity of perovskite-type oxides (Peña and Fierro, 2001; Smit et al., 2006). When the strain becomes larger than ultimate strain, the system is subject to attack by vacancy defects or high-temperature effects, etc., and the consequent collapse of crystal structures (Topsakal et al., 2010; Akhoundi et al., 2019).

Strain-Driven Spin-Arrangement Transition in $LaCoO_3$

Magnetic behaviors of materials arise from its spin arrangement. The results for the magnetic moment localized at Co atom (Mag_{Co}) under various strain (γ) are shown in **Figure 3A** and **Supplementary Tables S1, S2**. The main feature of the curve is that Mag_{Co} exhibits step-like change with strain in the calculated range from $\gamma = -4.0$ to 30%, reflecting low, intermediate, and high spin configurations. For strained $LaCoO_3$ with intermediate- and high-spin configurations, the magnetic moment of Co increases with strain. This positive correlation between magnetic moment and strain is a general behavior, which was observed in various materials (Kushima et al., 2010; Hsu et al., 2018; Zhao et al., 2020b). Given the slight variation in the magnetic moment over each terrace, we take the average values over the corresponding strain range as the DFT calculated Mag_{Co}, listed in **Table 1**. From **Figure 3A**, for $\gamma < 1.0\%$, system manifests non-magnetic behavior. As strain increases ($\gamma \geq 1.0\%$), $LaCoO_3$ becomes ferromagnetic. Within $\gamma = 1.0$–4.0%, the values of Mag_{Co} maintain at around 1.406 μ_B. When $\gamma \geq 4.0\%$, the average Mag_{Co} is 2.561 μ_B. Owing to the dependence of magnetic

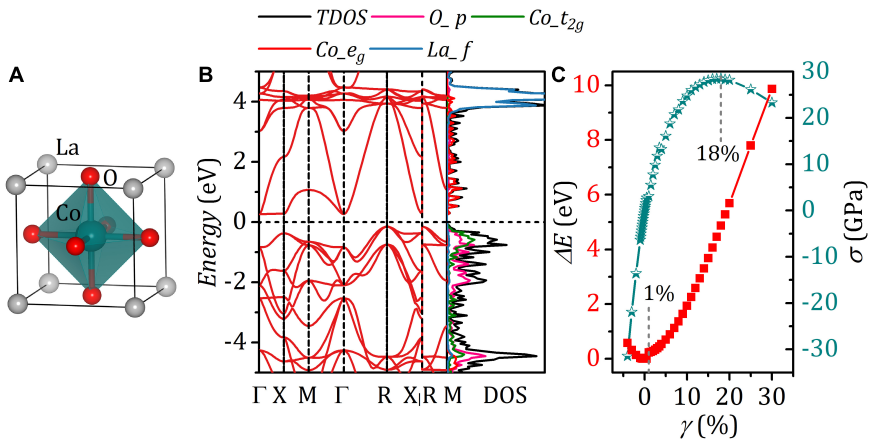

FIGURE 2 | (A) Crystal structure of $LaCoO_3$ and **(B)** corresponding band structure. **(C)** Strain energy of $LaCoO_3$ versus strain γ and strain–stress curve.

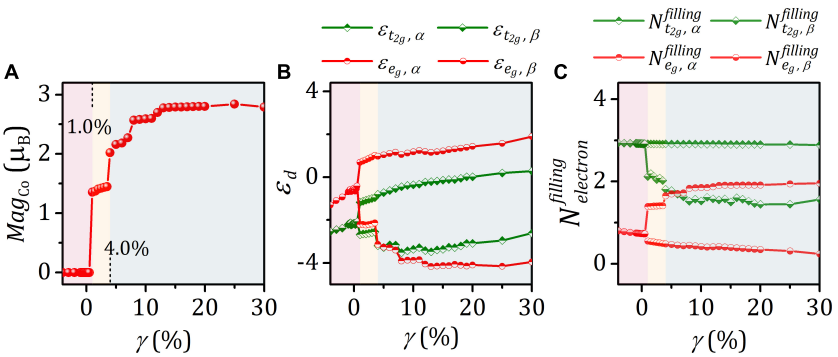

FIGURE 3 | (A–C) Magnetic moment localized at Co atom (Mag_{Co}), *d*-band center (ε_d), and *d*-band filling ($N^{filling}_{electron}$) versus strain γ.

moment on the U_{eff} parameter of the DFT+U method (Anisimov et al., 1991; Knížek et al., 2005), the calculated magnetic moments and actual magnetization values differ. Although a large U_{eff} value can be used to obtain the magnetic moment consistent with the experimental value, this would lead to the wrong estimation of the ground state energy (Tolba et al., 2018). To ensure the accuracy of results, we calculated the magnetic moments localized at Co atoms with U_{eff} = 3.0, 3.3, 3.5, 3.8, and 4.0 eV, for γ = 0.0, 2.0, and 8.0% (**Supplementary Table S1**). It is found that there is only a slight variation in the magnetic moment localized Co atom within the reasonable range of U_{eff} values (more information, see **Supplementary Table S1**), indicating the accuracy of our conclusion on the spin configuration transition. Furthermore, the previous theoretical investigation has shown that the strained $LaCoO_3$ has an intermediate-spin and high-spin configuration at a strain of 3 and 11%, respectively, which is consistent with the results in this work (Kushima et al., 2010).

To seek the physical origin of the step-like dependence of Mag_{Co} on the strain, we analyze the electronic structures by calculating the *d*-band center and corresponding orbital occupancy (**Figures 3B,C**; for detailed data, see **Supplementary Tables S2, S3**). It is observed that t_{2g} and e_g bands are spin-degenerate for $\gamma < 1.0\%$ (**Figure 3B**). However, in the case of $\gamma \geq 1.0\%$, the spin degeneracy is lifted, and the degenerate *d* bands split into two bands. The corresponding spin splitting is estimated by the gap of *d*-band center between the majority α-spin and minority β-spin, presented in **Figure 3B**. The spin splitting increases with γ. As compared with the t_{2g} band, the degree of spin splitting is significantly larger in e_g, which is accompanied by the change of the octahedral field splitting. The octahedral field splitting is assessed by the gap of *d*-band center between the t_{2g} and e_g with same spin states. It is noted that the predominant change of the octahedral field split concentrates in majority α–spin *d* orbitals. The majority α–spin t_{2g} and e_g band centers show step-like descent as γ increases. Especially, the majority α–spin e_g-band center becomes lower than the t_{2g}-band center when $\gamma \geq 4.0\%$. This indicates the smallest octahedral

TABLE 1 | Bond length, d_{Co-O} in Å and magnetic moment localized at Co atom, Mag_{Co} in μ_B of $LaCoO_3$.

Strain	d_{Co-O}	Mag_{Co}
$-4.0\% \leq \gamma < +1.0\%$	$1.829 \leq d_{Co-O} < 1.925$	0.000
$+1.0\% \leq \gamma < +4.0\%$	$1.925 \leq d_{Co-O} < 1.982$	1.406
$+4.0\% \leq \gamma < +18.0\%$	$1.982 \leq d_{Co-O} < 2.248$	2.561

field splitting occurs within $\gamma \geq 4.0\%$ compared with that in $\gamma < 1.0\%$ and $1.0\% \leq \gamma < 4.0\%$. These changes of crystal field splitting and spin splitting would affect orbital occupancy and accordingly magnetic moment. The fundamental origin of the change of octahedral field splitting is the change of the electrostatic interaction between Co and O with different Co–O bond length (d_{Co-O}). The low-spin, intermediate-spin, and high-spin configurations are in the range $d_{Co-O} < 1.925$ Å, 1.925 Å $\leq d_{Co-O} < 1.982$ Å, and $d_{Co-O} \geq 1.982$ Å, respectively (**Table 1**).

We further quantify the *d* band-filling numbers by integrating the projected densities of states with respect to energy up to the Fermi level. $N_{e_g,\,\alpha}^{filling}$, $N_{e_g,\,\beta}^{filling}$, $N_{t_{2g},\alpha}^{filling}$, and $N_{t_{2g},\,\beta}^{filling}$ were used to denote t_{2g} and e_g filling in different spin states. The corresponding data are listed in **Supplementary Table S3**. **Figure 3C** reveals that $N_{e_g,\,\alpha}^{filling}$ increases with strain. In contrast, the minority β-spin t_{2g} bands exhibit a reverse filling trend. The rise of majority α–spin e_g band-filling number results in the enhancement of magnetic moment and the transition of spin configuration. $N_{t_{2g},\alpha}^{filling}$ and $N_{e_g,\,\beta}^{filling}$ under strain were observed to be roughly constant. This follows from $3d^6$ electron configuration of trivalent Co ion and the *d*-orbital splitting under the octahedral field. The projected density of states of Co atoms (**Figures 4a–e**) indicates that with strain increasing the minority β–spin t_{2g} states shift upward with relative to Fermi level, whereas electrons gradually fill majority α–spin e_g states. Based on the analysis of the octahedral field, spin splitting, and *d*-orbital filling, we obtained low-spin, intermediate-spin, and high-spin arrangements in the corresponding octahedral field, illustrated in **Figures 4f–h**.

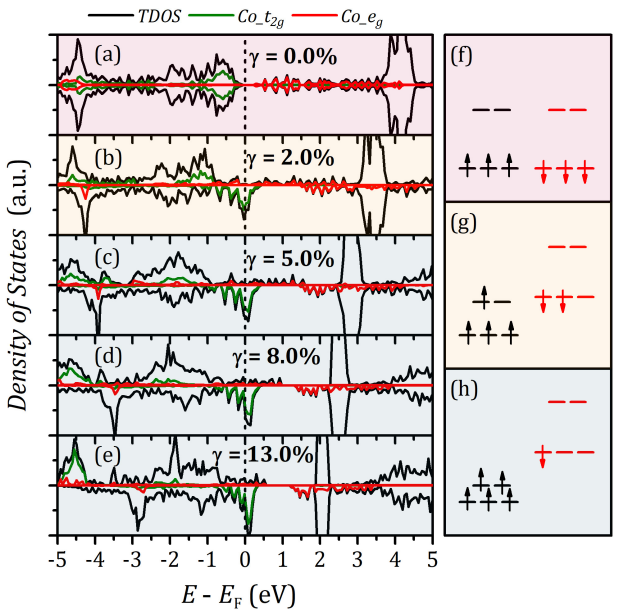

FIGURE 4 | Density of states of $LaCoO_3$ under various strain: **(a–e)** γ = 0.0, 2.0, 5.0, 8.0, and 13.0%. The schematic diagram of crystal field and corresponding spin arrangements: **(f)** low spin, **(g)** intermediate spin, and **(h)** high spin.

Effect of Ba Substitution in $LaCoO_3$ on Magnetic Properties

Strain could be achieved through introduction of defect or epitaxial substrate, etc. To apply tensile strain in $LaCoO_3$, we used Ba with a larger radius than La to partially replace La atom of $LaCoO_3$ (Ba^{2+}: 1.61 Å, La^{3+}: 1.36 Å) (Shannon, 1976). Nine possible configurations were considered based on the Ba content and the locations of Ba atoms: $La_{0.875}Ba_{0.125}CoO_3$ (Ba_c), $La_{0.75}Ba_{0.25}CoO_3$ (Ba_{c+b}), $La_{0.75}Ba_{0.25}CoO_3$ (Ba_{c+f1}, Ba_{c+f2}, Ba_{c+e1}, Ba_{c+e2}), $La_{0.625}Ba_{0.375}CoO_3$ ($Ba_{c+f1+f3}$, $Ba_{c+b\ +f1}$), and $La_{0.5}Ba_{0.5}CoO_3$($Ba_{c+f1+f2+f3}$) (see **Figure 5**). Here, *c*, *b*, *f*, and *e* denote corner, body center, face center, and edge center sites, respectively. Ba_c, Ba_{c+b}, and $Ba_{c+f1+f2+f3}$ denote Ba occupying the dispersive La sites to form Ba uniform-distributed structures (**Figure 5**). Other Ba substitutional defects distributed unevenly instead. The Ba substitutions can be formed due to the small substitutional energies of −0.356, −1.076, −1.083, −1.418, −1.415, −0.766, −1.076, 0.402, and 0.071 eV. The overall substitutional energies manifest the stability of the structure, reflecting the possibility of substituted perovskite compounds with the formula of $A_{1-x}A'_xB_{1-x}B'_xO_3$ (Peña and Fierro, 2001). In experiments, various $R_{1-x}A_xCoO_3$ (R = La, Pr, and Nd; A = Ba, Sr, and Ca), with *x* ranging from 0 to 0.5, have been successfully synthesized (Muta et al., 2002; Khalil, 2003; Masuda et al., 2003; Kun et al., 2013). For our investigated Ba substitution-modified $LaCoO_3$, the charge transfer of Ba is +1.552 to +1.577*e*, close to its formal charges of +2*e* (**Table 2**). The charge transfer of La approaches to its formal charge (+3*e*) with a value of about +2.0 *e*.

The consequence of the introduction of Ba substitution at La site causes the lattice expansions. In this work, the uniform distribution of Ba atoms promotes homogeneous elongation of lattice constants along with a, b, and c directions (Ba_c: $a_s = b_s = c_s = 0.96\%$; Ba_{c+b}: $a_s = b_s = c_s = 1.31\%$; $Ba_{c+f1+f3}$: $a_s = b_s = c_s = 1.74\%$; $Ba_{c+f1+f2+f3}$: $a_s = b_s = c_s = 2.05\%$) (**Figure 6A**). For the systems with uneven distributions of Ba atoms (Ba_{c+f1}, Ba_{c+f2}, Ba_{c+e1}, Ba_{c+e2}, and Ba_{c+b+f1}), especially Ba_{c+b+f1}, the structures derivate away from cubic symmetry (see **Figure 6A**), resulting in anisotropic physical properties of Co atoms. The lattice expansion-induced strain corresponds to the intermediate-spin strain range of defect-free $LaCoO_3$ (1.0–4.0%) (**Figure 6A**). The corresponding magnetic moments of each Co atoms are listed in **Table 2** and **Supplementary Table S4**. For Ba_{c+b+f1} substitutional defect modified $LaCoO_3$, the magnetic moments of Co atom are largely different, with an average value of 2.157 μ_b ranging from 1.606 to 2.761 μ_b (**Supplementary Table S4** and **Figure 6B**). In the case of slight deviation from cubic structures ($Ba_{c+f1/f2/e1/e2}$), Co atoms have the same magnetic moments (Ba_{c+f1}: 1.834 μ_b; Ba_{c+f2}: 1.836 μ_b; Ba_{c+e1}: 1.834 μ_b; Ba_{c+e2}: 1.833 μ_b) (**Figure 6B** and **Table 2**). For the systems with uniform Ba distribution, Ba_c, Ba_{c+b}, $Ba_{c+f1+f3}$, and $Ba_{c+f1+f2+f3}$, eight Co atoms in each structure are equivalent and possess the same magnetic moment (Ba_c: 2.111 μ_b;

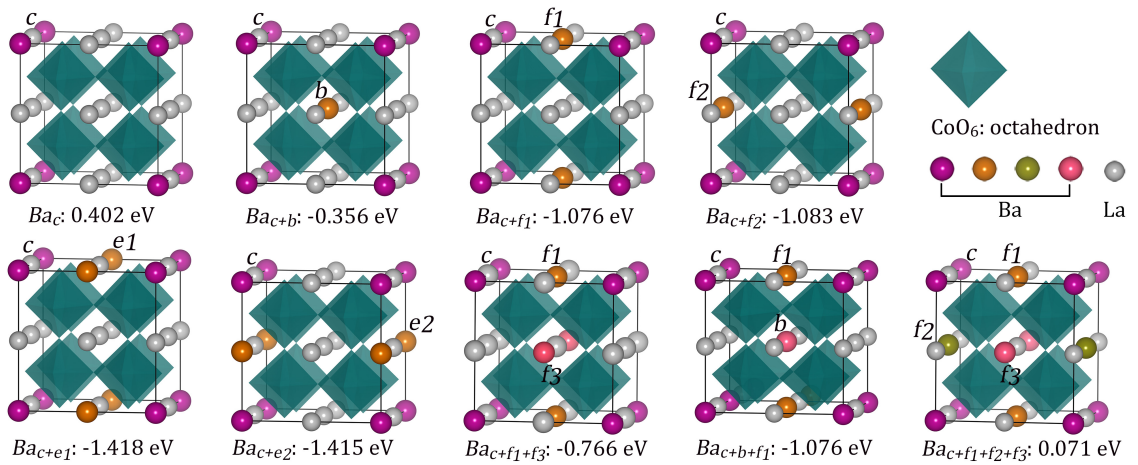

FIGURE 5 | Optimized structures of Ba-substituted $LaCoO_3$ and corresponding stabilization energies of Ba substitutional defects.

TABLE 2 | The magnetic moment localized at Co atom, Mag_{Co} in μ_B, charge transfer of Co atom, ΔQ^{Co}, $\Delta Q^{Co}_{wo\_strain}$ in *e*, and the charge transfer of La and Ba atom, ΔQ^{La}, ΔQ^{Ba} in *e*, for Ba_c, Ba_{c+b}, Ba_{c+f1}, Ba_{c+f2}, Ba_{c+e1}, Ba_{c+e2}, $Ba_{c+f1+f3}$, and $Ba_{c+f1+f2+f3}$ defective systems ($\Delta Q^{Co}_{wo\_strain}$ is the charge transfer of Co atom in defective $LaCoO_3$ due to the difference of electronic configuration between Ba and La).

Systems	Ba_c	Ba_{c+b}	Ba_{c+f1}	Ba_{c+f2}	Ba_{c+e1}	Ba_{c+e2}	$Ba_{c+f1+f3}$	$Ba_{c+f1+f2+f3}$
Mag_{Co}	2.109	2.365	1.835	1.837	1.834	1.833	1.916	2.197
ΔQ^{Co}	1.409	1.439	1.427	1.427	1.415	1.415	1.434	1.407
$\Delta Q^{Co}_{wo\_strain}$	0.105	0.126	0.035	0.035	0.040	0.041	0.048	0.111
ΔQ^{La}	2.105	2.095	2.096	2.096	2.109	2.107	2.116	2.097
ΔQ^{Ba}	1.577	1.557	1.560	1.557	1.563	1.562	1.554	1.552

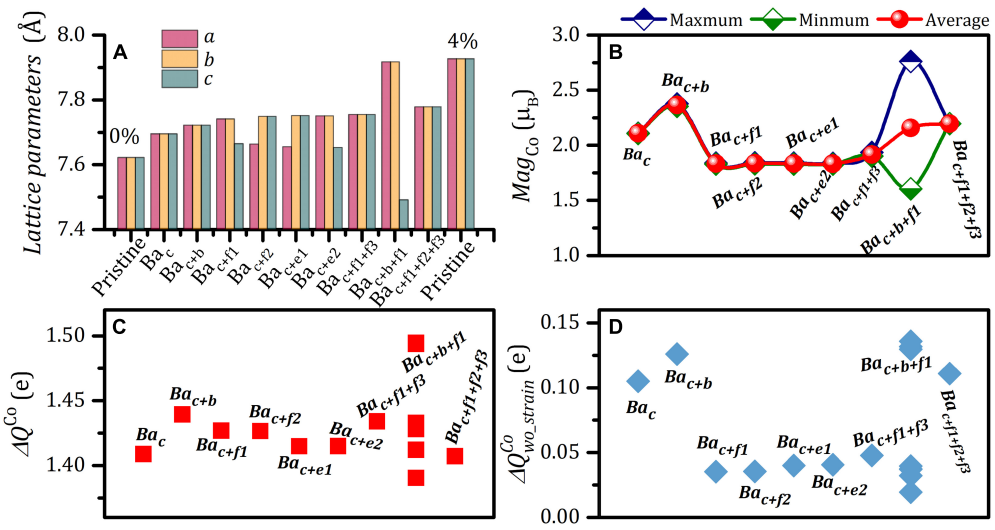

FIGURE 6 | (A) Lattice parameters along a, b, and c directions, **(B)** magnetic moment localized at Co atom (Mag_{Co}), **(C)** charge transfer of Co atom, and **(D)** charge transfer of Co atom excluding effect of variation in lattice in Ba-substituted $LaCoO_3$.

Ba_{c+b}: 2.377 μ_b; $Ba_{c+f1+f3}$: 1.936 μ_b; $Ba_{c+f1+f2+f3}$: 2.197 μ_b). Although the strain induced by Ba introduction is within the strain range of intermediate spin of defect-free $LaCoO_3$, the magnetic moments localized at Co atoms deviate from ~1.5 μ_b of the intermediate spin structures.

To uncover the fundamental origin of the difference of magnetic moments between Ba-substituted $LaCoO_3$ and defect-free intermediate-spin $LaCoO_3$, we further analyze the charge states of Co atoms in Ba substitution modified $LaCoO_3$. **Figures 6C,D** outline the total charge transfer of Co to adjacent

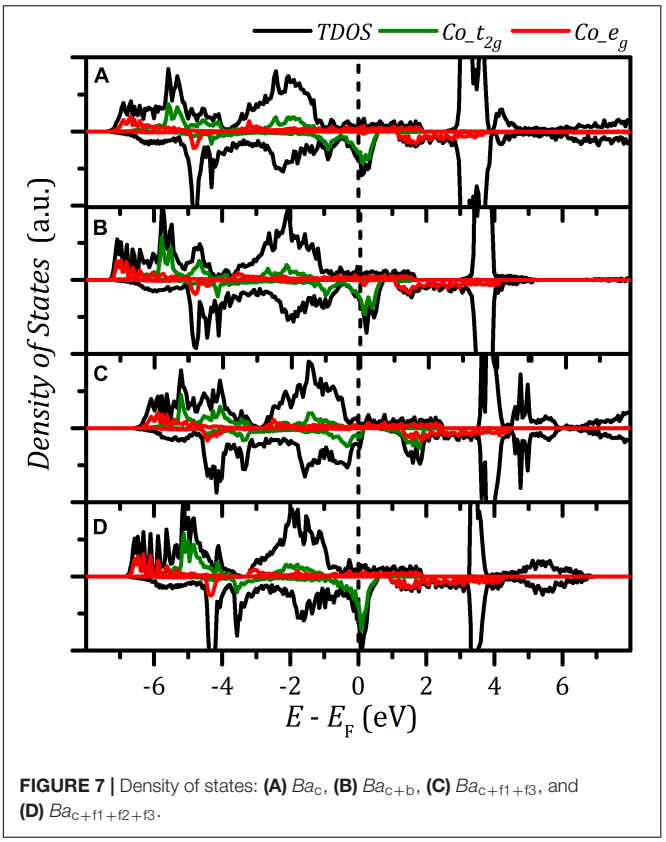

FIGURE 7 | Density of states: **(A)** Ba_c, **(B)** Ba_{c+b}, **(C)** $Ba_{c+f1+f3}$, and **(D)** $Ba_{c+f1+f2+f3}$.

O atoms, ΔQ^{Co} and the charge transfer of Co owing to the valence electronic configuration difference between Ba^{2+} and La^{3+}, $\Delta Q^{Co}_{wo\_strain}$, excluding the charge change resulting from lattice relaxation. The total charge transfer of Co atoms varies from +1.40 to +1.45*e*, differing from the value in strain-free $LaCoO_3$ (+1.335 *e*) (**Figure 6C**]. The Ba valence states indeed induced the variation in charge transfer of Co (**Figure 6D**). Specifically, for Ba_c, Ba_{c+b}, and $Ba_{c+f1+f2+f3}$ substitution modified $LaCoO_3$, $\Delta Q^{Co}_{wo\_strain}$ is 0.105, 0.126, and 0.111 *e*, respectively. As a comparison to these structures with uniform distribution of Ba atom, in the defective systems with Ba_{c+f1}, Ba_{c+f2}, Ba_{c+e1}, and Ba_{c+e2} substitutions, $\Delta Q^{Co}_{wo\_strain}$ dramatically decreases by 67–75% with values of 0.035–0.041*e*. It is a clear indication that the $\Delta Q^{Co}_{wo\_strain}$ is proportional to Mag_{Co} (e.g., Ba_{c+b}: $\Delta Q^{Co}_{wo\_strain}$ = 0.126*e*, Mag_{Co} = 2.365 μ_b; Ba_{c+f1}: $\Delta Q^{Co}_{wo\_strain}$ = 0.035*e*, Mag_{Co} = 1.835 μ_b) (**Figures 6B,D** and **Supplementary Figure S1**). Correspondingly, for $Ba_{c+f1+f3}$ substitution modified $LaCoO_3$, the small Mag_{Co} of 1.916 μ_b is accompanied by a small $\Delta Q^{Co}_{wo\_strain}$ of 0.048 *e*. For $Ba_{c,f1/f2/e1/e2}$ and $Ba_{c+f1+f3}$, the extremely small $\Delta Q^{Co}_{wo\_strain}$ of about 0.04*e* results in Mag_{Co} of ∼1.8 μ_b, which is well consistent with 1.5-μ_b magnetic moment of the pristine intermediate-spin configuration.

This effect of $\Delta Q^{Co}_{wo\_strain}$ on Mag_{Co} is further verified by the results of Ba_{c+b+f1} substitutional defect-modified $LaCoO_3$. For example, the large $\Delta Q^{Co}_{wo\_strain}$ on Co^2, Co^5, and Co^8 in Ba_{c+b+f1} substitution-modified $LaCoO_3$ (upper case digits on Co represent the different Co sites; see **Supplementary Figure S2** for details), are accompanied by large Mag_{Co} of 2.059, 2.757, and 2.758 μ_b (**Supplementary Table S4**). Meanwhile, the small Mag_{Co} of 1.781, 1.783, 1.606, and 1.752 μ_b are observed on Co^1, Co^4, Co^6, and Co^7 atoms associating with the corresponding small $\Delta Q^{Co}_{wo\_strain}$ of 0.037, 0.040, 0.037, and 0.020*e*. However, Co^3 atom in Ba_{c+b+f1}-modified $LaCoO_3$ is an abnormal case. The magnetic moment localized at Co^3 site is 2.761 μ_b despite the small $\Delta Q^{Co}_{wo\_strain}$ of 0.032*e*. Further analysis suggests that the charge transfer of Co^3 site, using the charge state of Co atom of pristine strain-free $LaCoO_3$ as benchmark, is 0.036*e*, which is almost the same as $\Delta Q^{Co}_{wo\_strain}$. Therefore, the valence state of Ba dominates the charge transfer in Co^3 site, eventually leads to large magnetic moment localized at Co^3 site. Overall, the Ba substitutional defect-modified $LaCoO_3$ possesses intermediate-spin configurations. The values of magnetic moments localized at Co atoms deviating from the 1.5 μ_b of pristine strained intermediate spin $LaCoO_3$ results from the different electronic configurations between Ba and La. And, the degree of deviation depends on the magnitude of the charge transfer of Co atoms following from the different valence states between Ba and La.

The projected density of states of Co atom reveals that the systems with Ba_c, Ba_{c+b}, and $Ba_{c+f1+f2+f3}$ substitutional defect hold similar orbital occupations, which differs from $Ba_{c+f1+f3}$ substitution modified $LaCoO_3$ (**Figures 7A–D**). The *d*-orbital filling exhibit that, for $Ba_{c+f1+f3}$, the minority β-spin t_{2g} filling increases accompanied by reducing majority α–spin e_g filling, compared with the defective $LaCoO_3$ including Ba_c, Ba_{c+b}, and $Ba_{c+f1+f2+f3}$ substituents (**Supplementary Figure S3**), which contributes to the small magnetic moment. The defective systems with a small magnetic moment, Ba_{c+f1}, Ba_{c+f2}, Ba_{c+e1}, and Ba_{c+e2}, have similar *d*-orbital occupation as $Ba_{c+f1+f3}$ (**Supplementary Figure S4**). All these features of *d*-orbital occupation are found in different Co atoms of $Ba_{c+f1+f3}$ substitution modified $LaCoO_3$ (**Supplementary Figure S5**). Ba substitutional defects induce a unit-like e_g occupancy resulting in a moderate interaction between Co active center and oxygen-related adsorbates, which contributes to the reduction of the OER/ORR thermodynamic overpotential. Therefore, Ba substitution defect modified $LaCoO_3$ is promising for oxygen redox catalytic reactions.

CONCLUSION

In summary, we explored the dependence of spin configurations on strain in $LaCoO_3$ via DFT calculations. We found that strain by manipulation lattice constants can tune crystal field splitting and spin splitting, resulting in the transition of spin arrangement. The important e_g unit occupancy was achieved via applying tri-axial uniform strain ranging from 1.0 to 4.0%. To achieve the strain effects practically, the substitution of La by Ba with larger ionic radius effectively introduces strain, leading to the unit-like occupancy of e_g. Notably, there is larger magnetic moment localized at Co atom in Ba substitution modified $LaCoO_3$ relative to the equivalent strained defect-free $LaCoO_3$, due to the lower

oxidation state of Ba than La. The response of spin configuration on strain induced by defect enables precise control of the unit occupancy of e_g during the catalyst design process.

DATA AVAILABILITY STATEMENT

The datasets generated for this study are available via the corresponding author or other researchers following publication.

AUTHOR CONTRIBUTIONS

LW performed the DFT calculations. LW, JL, and WW wrote this manuscript. WW administrated the project. MW provided the computational resources. HW, KL, YS, and ZL advised the research work.

FUNDING

This work was supported by the National Key Research and Development Program (Grant No. 2016YFB0901600), Tianjin City Distinguish Young Scholar Fund, National Natural Science Foundation of China (21573117 and 21975136), Tianjin Key Research and Development Program (Grant No. 18ZXSZSF00060), pen funds from National Engineering Lab for Mobile Source Emission Control Technology (NELMS2018A01), and the Fundamental Research Funds for the Central Universities (63185015).

SUPPLEMENTARY MATERIAL

The Supplementary Material for this article can be found online at: https://www.frontiersin.org/articles/10.3389/fmats.2020.00060/full#supplementary-material

REFERENCES

Abbate, M., Fuggle, J. C., Fujimori, A., Tjeng, L. H., Chen, C. T., Potze, R., et al. (1993). Electronic structure and spin-state transition of LaCoO3. *Phys. Rev. B-Condens Matter* 47, 16124–16130. doi: 10.1103/PhysRevB.47.16124

Akhoundi, E., Faghihnasiri, M., Memarzadeh, S., and Firouzian, A. H. (2019). Mechanical and strain-tunable electronic properties of the SnS monolayer. *J. Phys. Chem. Solids* 126, 43–54. doi: 10.1016/j.jpcs.2018.10.019

Anisimov, V. I., Zaanen, J., and Andersen, O. K. (1991). Band theory and Mott insulators: Hubbard U instead of Stoner I. *Phys. Rev. B* 44, 943–954. doi: 10.1103/PhysRevB.44.943

Arima, T., Tokura, Y., and Torrance, J. B. (1993). Variation of optical gaps in perovskite-type 3d transition-metal oxides. *Phys. Rev. B* 48, 17006–17009. doi: 10.1103/PhysRevB.48.17006

Asano, M., Kawamura, R., Sasakawa, R., Todoroki, N., and Wadayama, T. (2016). Oxygen reduction reaction activity for strain-controlled pt-based model alloy catalysts: surface strains and direct electronic effects induced by alloying elements. *ACS Catal.* 6, 5285–5289. doi: 10.1021/acscatal.6b01466

Chainani, A., Mathew, M., and Sarma, D. D. (1992). Electron-spectroscopy study of the semiconductor-metal transition in La1-xSrxCoO3. *Phys. Rev. B* 46, 9976–9983. doi: 10.1103/PhysRevB.46.9976

Duan, Y., Sun, S., Xi, S., Ren, X., Zhou, Y., Zhang, G., et al. (2017). Tailoring the Co 3d-O 2p covalency in LaCoO3 by Fe substitution to promote oxygen evolution reaction. *Chem. Mater.* 29, 10534–10541. doi: 10.1021/acs.chemmater.7b04534

Escudero-Escribano, M., Malacrida, P., Hansen, M. H., Vej-Hansen, U. G., Velázquez-Palenzuela, A., Tripkovic, V., et al. (2016). Tuning the activity of Pt alloy electrocatalysts by means of the lanthanide contraction. *Science* 352, 73–76. doi: 10.1126/science.aad8892

Escudero-Escribano, M., Verdaguer-Casadevall, A., Malacrida, P., Grønbjerg, U., Knudsen, B. P., Jepsen, A. K., et al. (2012). Pt5Gd as a highly active and stable catalyst for oxygen electroreduction. *J. Am. Chem. Soc.* 134, 16476–16479. doi: 10.1021/ja306348d

Freeland, J. W., Liu, J., Kareev, M., Gray, B., Kim, J. W., Ryan, P., et al. (2011). Orbital control in strained ultra-thin LaNiO3/LaAlO3 superlattices. *Europhys. Lett.* 96:57004. doi: 10.1209/0295-5075/96/57004

Ganguly, P., and Vasanthacharya, N. Y. (1986). Infrared and Mössbauer spectroscopic study of the metal-insulator transition in some oxides of perovskite structure. *J. Solid State Chem.* 61, 164–170. doi: 10.1016/0022-4596(86)90018-6

Gani, T. Z. H., and Kulik, H. J. (2018). Understanding and breaking scaling relations in single-site catalysis: methane to methanol conversion by FeIV=O. *ACS Catal.* 8, 975–986. doi: 10.1021/acscatal.7b03597

Hammer, B., Morikawa, Y., and Nørskov, J. K. (1996). CO chemisorption at metal surfaces and overlayers. *Phys. Rev. Lett.* 76, 2141–2144. doi: 10.1103/PhysRevLett.76.2141

Hammer, B., Nielsen, O. H., and Nrskov, J. K. (1997). Structure sensitivity in adsorption: CO interaction with stepped and reconstructed Pt surfaces. *Catal. Lett.* 46, 31–35. doi: 10.1023/A:1019073208575

Hammer, B., and Norskov, J. K. (2000). Theoretical surface science and catalysis - calculations and concepts. *Adv. Catal.* 45, 71–129. doi: 10.1021/acs.accounts.8b00399

Holmblad, P. M., Larsen, J. H., Chorkendorff, I., Nielsen, L. P., Besenbacher, F., Stensgaard, I., et al. (1996). Designing surface alloys with specific active sites. *Catal. Lett.* 40, 131–135. doi: 10.1007/BF00815272

Hong, W. T., Risch, M., Stoerzinger, K. A., Grimaud, A., Suntivich, J., and Shao-Horn, Y. (2015). Toward the rational design of non-precious transition metal oxides for oxygen electrocatalysis. *Energy Environ. Sci.* 8, 1404–1427. doi: 10.1039/C4EE03869J

Hsu, S.-H., Hung, S.-F., Wang, H.-Y., Xiao, F.-X., Zhang, L., Yang, H., et al. (2018). Tuning the electronic spin state of catalysts by strain control for highly efficient water electrolysis. *Small Methods* 2:1800001. doi: 10.1002/smtd.201800001

Jiang, M., Li, J., Zhao, Y., Pan, L., Cao, Q., Wang, D., et al. (2018). Double perovskites as model bifunctional catalysts toward rational design: the correlation between electrocatalytic activity and complex spin configuration. *ACS Appl. Mater. Interfaces* 10, 19746–19754. doi: 10.1021/acsami.8b05353

Khalil, M. S. (2003). Synthesis, X-ray, infrared spectra and electrical conductivity of La/Ba–CoO3 systems. *Mater. Sci. Eng. A* 352, 64–70. doi: 10.1016/s0921-5093(02)00557-9

Knížek, K., Novák, P., and Jirák, Z. (2005). Spin state of LaCoO3: dependence on CoO6 octahedra geometry. *Phys. Rev. B* 71:054420. doi: 10.1103/PhysRevB.71.054420

Kratzer, P., Hammer, B., and Nørskov, J. K. (1996). Geometric and electronic factors determining the differences in reactivity of H2 on Cu(100) and Cu(111). *Surf. Sci.* 359, 45–53. doi: 10.1016/0039-6028(96)00309-3

Kresse, G., and Furthmüller, J. (1996). Efficient iterative schemes for ab initio total-energy calculations using a plane-wave basis set. *Phys. Rev. B* 54, 11169–11186. doi: 10.1103/PhysRevB.54.11169

Kresse, G., and Joubert, D. (1999). From ultrasoft pseudopotentials to the projector augmented-wave method. *Phys. Rev. B* 59, 1758–1775. doi: 10.1103/PhysRevB.59.1758

Kun, R., Populoh, S., Karvonen, L., Gumbert, J., Weidenkaff, A., and Busse, M. (2013). Structural and thermoelectric characterization of Ba substituted LaCoO3 perovskite-type materials obtained by polymerized gel combustion method. *J. Alloys Compd.* 579, 147–155. doi: 10.1016/j.jallcom.2013.05.019

Kushima, A., Yip, S., and Yildiz, B. (2010). Competing strain effects in reactivity of LaCoO3 with oxygen. *Phys. Rev. B* 82:115435. doi: 10.1103/PhysRevB.82.115435

Kuznetsov, D. A., Han, B., Yu, Y., Rao, R. R., Hwang, J., Román-Leshkov, Y., et al. (2018). Tuning redox transitions via inductive effect in metal oxides and complexes, and implications in oxygen electrocatalysis. *Joule* 2, 225–244. doi: 10.1016/j.joule.2017.11.014

Li, H.-B., Yang, Z., Liu, J., Yao, X., Xiong, K., Liu, H., et al. (2016). Electronic properties and native point defects of high efficient NO oxidation catalysts SmMn2O5. *Appl. Phys. Lett.* 109:211903. doi: 10.1063/1.4968786

Liu, H. Y., Yan, R. X., Zhang, R. G., Wang, B. J., and Xie, K. C. (2011). A DFT theoretical study of CH4 dissociation on gold-alloyed Ni(111) surface. *J. Nat. Gas Chem.* 20, 611–617. doi: 10.1016/s1003-9953(10)60252-6

Maitra, U., Naidu, B. S., Govindaraj, A., and Rao, C. N. R. (2013). Importance of trivalency and the eg1 configuration in the photocatalytic oxidation of water by Mn and Co oxides. *Proc. Natl. Acad. Sci. U. S. A.* 110, 11704–11707. doi: 10.1073/pnas.1310703110

Masuda, H., Fujita, T., Miyashita, T., Soda, M., Yasui, Y., Kobayashi, Y., et al. (2003). Transport and magnetic properties of R1-xAxCoO3 (R = La, Pr and Nd; A = Ba, Sr and Ca). *J. Phys. Soc. Jpn.* 72, 873–878. doi: 10.1143/JPSJ.72.873

Matsumoto, Y., Yoneyama, H., and Tamura, H. (1977a). Catalytic activity for electrochemical reduction of oxygen of lanthanum nickel oxide and related oxides. *J. Electroanal. Chem. Interfacial Electrochem.* 79, 319–326. doi: 10.1016/s0022-0728(77)80453-1

Matsumoto, Y., Yoneyama, H., and Tamura, H. (1977b). Influence of the nature of the conduction band of transition metal oxides on catalytic activity for oxygen reduction. *J. Electroanal. Chem. Interfacial Electrochem.* 83, 237–243. doi: 10.1016/s0022-0728(77)80169-1

Mavrikakis, M., Hammer, B., and Norskov, J. K. (1998). Effect of strain on the reactivity of metal surfaces. *Phys. Rev. Lett.* 81, 2819–2822. doi: 10.1103/PhysRevLett.81.2819

Muta, K., Kobayashi, Y., and Asai, K. (2002). Magnetic, electronic transport, and calorimetric investigations of La1-xCaxCoO3 in comparison with La1-xSrxCoO3. *J. Phys. Soc. Jpn.* 71, 2784–2791. doi: 10.1143/JPSJ.71.2784

Peña, M. A., and Fierro, J. L. G. (2001). Chemical structures and performance of perovskite oxides. *Chem. Rev.* 101, 1981–2018. doi: 10.1021/cr980129f

Perdew, J. P., Burke, K., and Ernzerhof, M. (1996). Generalized gradient approximation made simple. *Phys. Rev. Lett.* 77, 3865–3868. doi: 10.1103/PhysRevLett.77.3865

Pesquera, D., Herranz, G., Barla, A., Pellegrin, E., Bondino, F., Magnano, E., et al. (2012). Surface symmetry-breaking and strain effects on orbital occupancy in transition metal perovskite epitaxial films. *Nat. Commun.* 3:1189. doi: 10.1038/ncomms2189

Rivadulla, F., Bi, Z., Bauer, E., Rivas-Murias, B., Vila-Fungueiriño, J. M., and Jia, Q. (2013). Strain-induced ferromagnetism and magnetoresistance in epitaxial thin films of LaCoO3 prepared by polymer-assisted deposition. *Chem. Mater.* 25, 55–58. doi: 10.1021/cm3031472

Shannon, R. (1976). Revised effective ionic radii and systematic studies of interatomic distances in halides and chalcogenides. *Acta Crystallogr. Sect. A* 32, 751–767. doi: 10.1107/S0567739476001551

Smit, J. P., Stair, P. C., and Poeppelmeier, K. R. (2006). The adaptable lyonsite structure. *Chem.-Eur. J.* 12, 5944–5953. doi: 10.1002/chem.200600294

Strasser, P., Koh, S., Anniyev, T., Greeley, J., More, K., Yu, C., et al. (2010). Lattice-strain control of the activity in dealloyed core–shell fuel cell catalysts. *Nat. Chem.* 2, 454–460. doi: 10.1038/nchem.623

Suntivich, J., Gasteiger, H. A., Yabuuchi, N., Nakanishi, H., Goodenough, J. B., and Shao-Horn, Y. (2011a). Design principles for oxygen-reduction activity on perovskite oxide catalysts for fuel cells and metal–air batteries. *Nat. Chem.* 3, 546–550. doi: 10.1038/nchem.1069

Suntivich, J., May, K. J., Gasteiger, H. A., Goodenough, J. B., and Shao-Horn, Y. (2011b). A perovskite oxide optimized for oxygen evolution catalysis from molecular orbital principles. *Science* 334, 1383–1385. doi: 10.1126/science.1212858

Tolba, S. A., Gameel, K. M., Ali, B. A., Almossalami, H. A., and Allam, N. K. (2018). "The DFT+U: approaches, accuracy, and applications," in *Density Functional Calculations - Recent Progresses of Theory and Application*, ed. G. Yang, (London: IntechOpen).

Topsakal, M., Cahangirov, S., and Ciraci, S. (2010). The response of mechanical and electronic properties of graphane to the elastic strain. *Appl. Phys. Lett.* 96:091912. doi: 10.1063/1.3353968

Wang, L., Chen, H., and Wang, W. (2019a). N–H bond activation in ammonia by TM-SSZ-13 (Fe, Co, Ni and Cu) zeolites: a first-principles calculation. *Phys. Chem. Chem. Phys.* 21, 1506–1513. doi: 10.1039/C8CP06263C

Wang, L., Zeng, Z., Gao, W., Maxson, T., Raciti, D., Giroux, M., et al. (2019b). Tunable intrinsic strain in two-dimensional transition metal electrocatalysts. *Science* 363, 870–874. doi: 10.1126/science.aat8051

Wei, C., Feng, Z., Scherer, G. G., Barber, J., Shao-Horn, Y., and Xu, Z. J. (2017). Cations in octahedral sites: a descriptor for oxygen electrocatalysis on transition-metal spinels. *Adv. Mater.* 29:1606800. doi: 10.1002/adma.201606800

Xu, Y., Jiang, S.-X., Yin, W.-J., Sheng, W., Wu, L.-X., Nie, G.-Z., et al. (2020). Adsorption behaviors of HCN, SO2, H2S and NO molecules on graphitic carbon nitride with Mo atom decoration. *Appl. Surf. Sci.* 501:144199. doi: 10.1016/j.apsusc.2019.144199

Zhang, T., Li, H., Yang, Z., Cao, F., Li, L., Chen, H., et al. (2019). Electrospun YMn2O5 nanofibers: a highly catalytic activity for NO oxidation. *Appl. Catal. B: Environ.* 247, 133–141. doi: 10.1016/j.apcatb.2019.02.005

Zhao, G., Cheng, Y., Sun, P., Ma, W., Hao, S., Wang, X., et al. (2020a). Biocarbon based template synthesis of uniform lamellar MoS2 nanoflowers with excellent energy storage performance in lithium-ion battery and supercapacitors. *Electrochim. Acta* 331:135262. doi: 10.1016/j.electacta.2019.135262

Zhao, Y., Li, Y., Liu, M., Xu, K., and Ma, F. (2020b). Strain-controllable phase and magnetism transitions in Re-Doped MoTe2 monolayer. *J. Phys. Chem. C.* 124, 4299–4307. doi: 10.1021/acs.jpcc.9b11036

Zhao, G., Cheng, Y., Wu, Y., Xu, X., and Hao, X. (2018). New 2D carbon nitride organic materials synthesis with huge-application prospects in CN photocatalyst. *Small* 14:e1704138. doi: 10.1002/smll.201704138

Zhao, G., Wang, A., He, W., Xing, Y., and Xu, X. (2019). 2D new nonmetal photocatalyst of sulfur-doped h-BN nanosheeets with high photocatalytic activity. *Adv. Mater. Interfaces* 6:1900062. doi: 10.1002/admi.201900062

Zhou, S., Miao, X., Zhao, X., Ma, C., Qiu, Y., Hu, Z., et al. (2016). Engineering electrocatalytic activity in nanosized perovskite cobaltite through surface spin-state transition. *Nat. Commun.* 7:11510. doi: 10.1038/ncomms11510

Conflict of Interest: The authors declare that the research was conducted in the absence of any commercial or financial relationships that could be construed as a potential conflict of interest.